JOURNAL OF GEOPHYSICAL RESEARCH: OCEANS, VOL. 118, 5720–5731, doi:10.1002/jgrc.20415, 2013

Mesoscale eddies in the South Atlantic Bight

Renato M. Castelao[1] and Ruoying He[2]

Received 12 April 2013; revised 24 September 2013; accepted 25 September 2013; published 22 October 2013.

[1] Satellite-derived sea level anomaly fields constructed by combining measurements from simultaneously operating altimeters are used to quantify properties and propagation characteristics of eddies in the South Atlantic Bight (SAB). Eddy detection and eddy tracking algorithms are applied to 19 years of high-resolution observations available at weekly intervals. Inshore of the 800 m isobath, eddies are most frequently observed at and downstream of the Charleston Bump (a major topographic feature located at 31–32°N), a region where the amplitude of most eddies is increased. The bump is also a preferred region for eddy generation. The amplitude of eddies is found to increase with water depth. Eddies generated in the SAB tend to propagate westward toward the coast and to the northeast, presumably due to the influence of the strong mean northeastward flow of the Gulf Stream. Those eddies are highly nonlinear, with potential to trap water in their interior as they propagate. Since a large fraction of the eddies that at some point in their histories are found inshore of the 800 m isobath experience large bathymetric changes along their trajectories, they can potentially serve as efficient mechanisms for cross-isobath transport in the SAB. Analysis of temporal variability in eddy activity suggests that cross-isobath transport due to nonlinear eddies may be significant during all seasons, but will likely be characterized by large interannual variability.

Citation: Castelao, R. M., and R. He (2013), Mesoscale eddies in the South Atlantic Bight, *J. Geophys. Res. Oceans*, *118*, 5720–5731, doi:10.1002/jgrc.20415.

1. Introduction

[2] Mesoscale eddies are ubiquitous features in the oceans, playing a substantial role in the transfer of energy and water properties across different spatial and temporal scales [*Chaigneau et al*., 2009]. They are known to influence the distribution of physical [e.g., *Atkinson and Blanton*, 1986; *Lagerloef*, 1992], chemical [e.g., *Lee et al*., 1991], and biogeochemical [e.g., *Oschlies and Garçon*, 1998] properties in the ocean. Vertical fluxes of nutrients induced by the dynamics of mesoscale eddies in the open ocean have been shown to supply a large fraction of the annual nutrient requirement to sustain observed rates of new production [*McGillicudy et al*., 1998].

[3] Satellite observations of sea level anomalies (SLA) have revealed many eddy characteristics at global scale. In particular, observations have shown that mesoscale variability in the ocean occurs primarily as nonlinear vortices or eddies [*Chelton et al*., 2007, 2011b], which in contrast to linear waves can transport momentum, heat, mass, and the chemical constituents of seawater and therefore contribute to water mass distributions and ocean biology [*Robinson*, 1983]. Eddies have been shown to generate much of the observed variability in chlorophyll over the open ocean by passively advecting phytoplankton [*Chelton et al*., 2011a]. They have also been shown to suppress production in the highly productive eastern boundary upwelling systems because of eddy-induced transport of nutrients from the nearshore environment to the open ocean [*Gruber et al*., 2011]. While dampening productivity near the coast, eddy advection and diffusion can transfer nutrients from upwelling sites to neighboring areas [e.g., *Lee and Williams*, 2000], behaving as isolated oases of enhanced marine productivity in an otherwise nutrient-poor open ocean environment [*Crawford et al*., 2007]. Eddies have also been shown to transport plumes of suspended sediments from continental shelves into the deep ocean [*Washburn et al*., 1993].

[4] Off the U.S. Southeast coast at the South Atlantic Bight (SAB; we refer to SAB as the area shown in Figure 1, between Cape Canaveral and Cape Hatteras), eddies are thought to serve as major players enhancing shelf-slope exchange. Previous observations have revealed that cold-core cyclonic eddies observed on the Gulf Stream front are often associated with intense upwelling and consequently enhanced cross-isobath transport [*Lee et al*., 1991]. In particular, summer upwelling induced by the passage of the cold-core eddies often extend to midshelf or inner shelf if additional upwelling and onshore bottom transport is generated at the same time by upwelling favorable wind forcing [*Atkinson et al*., 1987; *Lee and Pietrafesa*, 1987;

[1]Department of Marine Sciences, University of Georgia, Athens, Georgia, USA.
[2]Department of Marine, Earth and Atmospheric Sciences, North Carolina State University, Raleigh, North Carolina, USA.

Corresponding author: R. M. Castelao, Department of Marine Sciences, University of Georgia, Marine Sciences Building, Athens, GA 30602, USA. (castelao@uga.edu)

2169-9275/13/10.1002/jgrc.20415

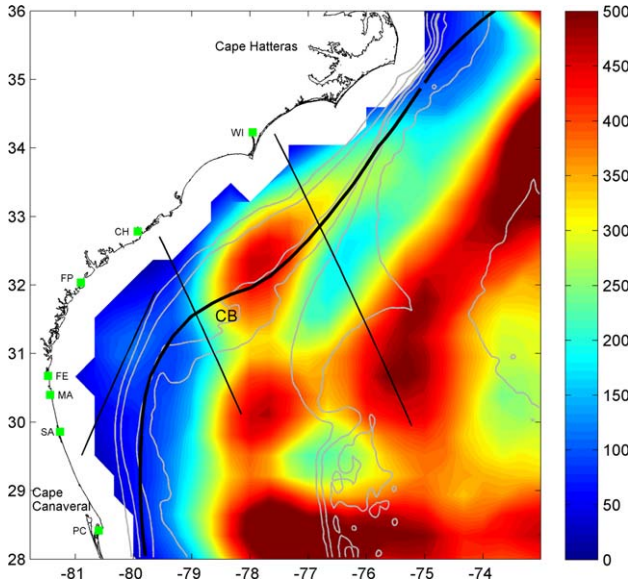

Figure 1. Number of eddies observed in 19 years of observations from satellite altimeters. Thick black line is a contour of mean dynamic topography, which shows the long-term average position of the core of the Gulf Stream. Black straight thinner lines are inner portions of three satellite tracks from Jason 1. The 60, 200, 600, 800, 1500, 3000, and 5000 m isobaths are shown in gray. CB stands for Charleston Bump. Locations of tide gauges used to detect the width of the coastal region where satellite observations are not reliable are shown in green. WI: Wilmington, NC; CH: Charleston, SC; FP: Fort Pulaski, GA; FE: Fernandina Beach, FL; MA: Mayport, FL; SA: St. Augustine, FL; PC: Port Canaveral, FL.

Aretxabaleta et al., 2006; *Hyun and He*, 2010; *Castelao*, 2011]. Additionally, Gulf Stream eddies can serve as conduits for coastal water leakage into the western boundary current [*Atkinson et al*., 1978; *Blanton and Pietrafesa*, 1978] and they play an important role determining the flux of heat, salt, nutrients, and carbon between the coastal and the deep ocean [*Lee et al*., 1981; *Lee and Atkinson*, 1983; *Atkinson et al*., 1987; *Lee et al*., 1991].

[5] Satellite altimetry provides a unique opportunity to investigate eddies in the SAB, with SLA data available for the last 20 years or so. This is especially true with the availability of satellite-derived SLA fields constructed by combining measurements from simultaneously operating altimeters [*Ducet et al*., 2000; *Le Traon et al*., 2003]. The combined products are of much higher resolution than SLA fields constructed from TOPEX/POSEIDON (T/P) data alone, enabling observational studies of mesoscale variability that were not previously possible using altimetry data [*Chelton et al*., 2011b]. Here we apply recently developed eddy detection and eddy tracking algorithms to those high resolution SLA fields to identify properties and propagation characteristics of eddies in the SAB as well as their potential for driving cross-isobath transport and shelf-slope exchange.

2. Methods

[6] Gridded sea level anomalies (SLA) fields analyzed here were constructed by SSALTO/DUACS at 7 day intervals with 1/3° resolution using measurements from simultaneously operating altimeters. The observations are distributed by AVISO (Archiving, Validation, and Interpretation of Satellite Oceanographic data) as the "Reference Series," which is built by combining data from a constant number (i.e., two) of altimeters over the entire time period. Even though using more altimeters whenever they are available could increase the quality of the observations during that period [*Pascual et al*., 2006], the accuracy and resolution of the observations would not be homogeneous through time [*Chelton et al*., 2011b]. In that case, low-frequency variability in eddy characteristics could also be a function of the number of altimeters observing the ocean at the time, instead of only a function of ocean dynamics. Eddies with e-folding scales smaller than 0.4° (zonal scale of about 35–40 km for the SAB latitudinal range) are filtered out of the objective analyses procedure implemented by SSALTO/DUACS, while those between 0.4° and 0.6° are attenuated [*Chelton et al*., 2011b]. Hydrographic observations from the National Oceanographic Data Center (NODC) processed as in *Castelao* [2011] were used to estimate the internal Rossby radius of deformation in the area by solving the vertical mode problem [*Kundu et al*., 1975]. The local value of the internal Rossby radius being 5–35 km implies that some of the eddies in the submesoscale/mesoscale range may not be well represented.

[7] We applied the eddy detection and eddy tracking algorithms described in *Chelton et al*. [2011b] to SLA observations from 14 October 1992 to 28 September 2011. Briefly, for each map of SLA, we look for regions (i.e., a set of connected pixels) that contain a local maximum (minimum) in SLA, and where all of the pixels in the region are above (below) a given SLA threshold for anticyclonic (cyclonic) eddies. Cyclonic and anticyclonic eddies are identified separately, and the SLA field is partitioned using a range of thresholds from -100 cm to $+100$ cm, proceeding upward in increments of 1 cm for anticyclonic eddies and downward for cyclonic eddies until a closed contour of SLA that satisfies the criteria above is found. This makes the algorithm "threshold-free" and capable of handling situations where an eddy is embedded in large scale background sea surface height variations [*Chelton et al*., 2011b]. After eddies were identified in each SLA map, the *Chelton et al*. [2011b] eddy tracking algorithm was used to determine the trajectory of each eddy. Specifically, for each eddy identified at time step k, the eddies identified at the next time step $k+1$ are searched to find the closest eddy lying within a circle with radius of 150 km and with amplitude and area that fall between 0.25 and 2.5 times those of the reference eddy being considered. If such an eddy is found, it is associated with the trajectory of the reference eddy at time k. Details of the eddy detection and eddy tracking algorithms can be found in *Chelton et al*. [2011b]. Eddies that could only be tracked for <4 weeks were discarded from subsequent analyses to reduce the risk of spurious eddies arising from noise in the SLA fields. The 4 week lifetime is commensurate with the 35 day e-folding time scale of the Gaussian covariance function in the objective analysis procedure used to construct the SLA fields of the AVISO Reference Series [*Chelton et al*., 2011b].

[8] Eddy characteristics were also defined as in *Chelton et al*. [2011b]. The amplitude of an eddy is computed as the

difference between the maximum (minimum) SLA within the anticyclonic (cyclonic) eddy and the average SLA around the outermost closed contour of SLA that defines the eddy perimeter. The eddy radius is the radius of the circle that has the same area as the region within the eddy perimeter. The rotational speed U of an eddy is characterized by the maximum of the average geostrophic speeds around all of the closed contours of SLA inside the eddy. We obtain a second estimate of the eddy spatial scale by computing the radius of the circle that has the same area as the region within the closed contour of SLA with maximum average rotational speed U.

[9] It is well known that satellite surface elevation observations near the coast are less reliable because of intrinsic difficulties in the various corrections applied to altimeter data in those regions [e.g., *Volkov et al*., 2007; *Saraceno et al*., 2008]. Therefore, observations near the coast are discarded before using the eddy detection and eddy tracking algorithms described above. The width of the region in which observations should be discarded was determined following the method used by *Saraceno et al*. [2008] using along-track satellite altimeter data from Jason-1, which is also distributed by AVISO. Briefly, the fraction of data available at each along-track position was determined as a function of distance from the coast. A substantial drop in the percentage of data available was observed at distances shorter than 40 km from the coast. This is similar to the 37 km wide coastal gap in reliable observations found off Oregon by *Saraceno et al*. [2008]. Observations collected at distances greater than 40 km from the coast were compared with tide gauge data obtained from the University of Hawaii Sea Level Center (see Figure 1 for location of tide gauges and altimeter tracks). Tide gauge data were low-pass filtered (half-power point of 40 h) to remove short-period fluctuations and corrected for the inverse barometer effect using the 6 h reanalysis of Sea Level Pressure produced by the National Centers for Environmental Prediction (NCEP). The tide gauge data were then low-pass filtered (half-power point of 20 days) to match the Nyquist frequency of the altimeter data. Sea level anomalies were estimated by subtracting the time average of the common record length at each point in the along-track altimeter data and at the tide gauges. Observations at distances greater than 40 km from the coast from the three tracks shown in Figure 1 were then correlated to observations from the tide gauges closest to the tracks (WI, CH, and SA, see Figure 1). In all three cases, the correlations are large and statistically significant (at the 95% confidence level) at ~40 km from the coast, decreasing slowly along the altimeter track as the distances to the tide gauges increase. At 40 km from the coast, correlation coefficients were 0.62, 0.77, and 0.87 from north to south. Analyses were repeated without correcting the tide gauge observations for the inverse barometer effect and correlations were also found to be statistically significant at 0.67, 0.82, and 0.87 (WI, CH, and SA, respectively). If we further high-pass filter the satellite and tide gauge observations to remove seasonal and interannual variability (half-power point of 120 days), correlations coefficients are 0.49, 0.63, and 0.68 when the observations are corrected for the inverse barometer effect, and 0.54, 0.69, and 0.67 for the noncorrected observations. In all cases, correlations are statistically significant at the 95% confidence level. To further confirm that observations farther than 40 km from the coast are reliable, tide gauge data (not corrected for the inverse barometer effect) from all gauges shown in Figure 1 were correlated to SLA observations from the gridded product described above that were located closest to the gauges but at least 40 km from the coast. Correlation coefficients, from north to south, were 0.69, 0.89, 0.83, 0.86, 0.90, 0.93, and 0.85 (all significant at the 95% confidence level). When the high-pass filtered (half-power point of 120 days) satellite and tide gauge observations are used, so that seasonal and interannual variability are removed, correlations coefficients, from north to south, drop to 0.57, 0.78, 0.63, 0.73, 0.64, 0.72, and 0.71, but still remain statistically significant (at the 95% confidence level). In summary, the analysis reveals that altimeter observations in the region are often missing inshore of 40 km from the coast. Offshore of 40 km from the coast, on the other hand, few observations (~10%) are missing and altimeter data is highly correlated with tide gauge observations. Therefore, we follow *Saraceno et al*. [2008] and eliminate all the gridded data estimated by AVISO that fall within 40 km from the coast. Gridded mean dynamic topography for the 1993–1999 period, also distributed by AVISO, is used in Figure 1 to identify the mean position of the Gulf Stream (i.e., the contour coinciding with the strongest mean dynamic topography gradient).

[10] Long-term observations of the Gulf Stream transport off the coast of Florida (approximately at 26.5°N, between Florida and the Grand Bahama Island at the Bahamas) were obtained by NOAA's Western Boundary Time Series project using a submarine cable and snapshot estimates made by shipboard instruments. Wind observations were obtained from the National Center for Environmental Prediction—National Center for Atmospheric Research Reanalysis. The coordinate system for the wind data was rotated so that the alongshelf component of the wind stress is aligned with the direction of isobaths to the northeast of the Charleston Bump (Figure 1). Alongshelf wind stress anomalies were determined by removing the seasonal cycle from the original time series.

3. Results

3.1. Eddy Characteristics

[11] The distribution of the number of eddies observed during the 19 year period extending from October 1992 to September 2011 is shown in Figure 1. To identify regions of high eddy activity, the frequency of eddy occurrence is calculated. The frequency of eddy occurrence at a given location is defined as the percentage of time that the point is located within an eddy (i.e., the distance between a given location and an eddy centroid is smaller than the eddy radius, e.g., *Chaigneau et al*. [2008, 2009]). There is substantial spatial variability in the frequency of eddy occurrence in the SAB (Figure 2). Cyclonic and anticyclonic eddies are more frequently observed offshore of the 800 m isobath, between 15% and 30% of the time on average. Inshore of the 800 m isobath, the frequency of eddy occurrence is generally smaller, especially south of 31°N. Between 32°N and 34°N, however, relatively high frequency of eddy occurrence is observed much closer to the coast, reaching inshore of the 60 m isobath. In particular,

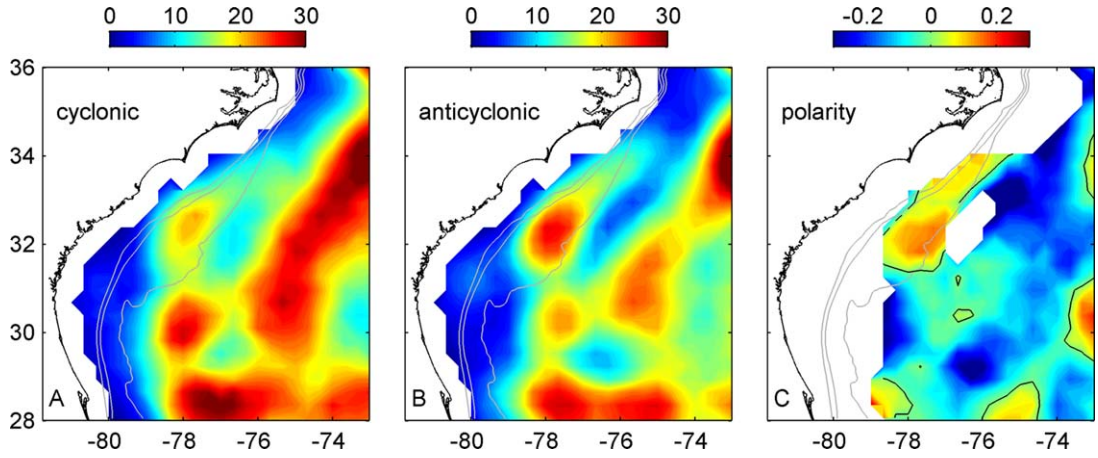

Figure 2. Frequency of occurrence (percentage of time that eddies are observed at a given location) of (a) cyclonic and (b) anticyclonic eddies with lifetime ≥4 weeks. (c) Polarity (see text for definition) for eddies with lifetime ≥4 weeks is also shown, where the black line is the zero contour. Polarity is only shown in regions where the frequency of eddy occurrence (cyclonic and anticyclonic) exceeds 20%. Gray contours are the 60, 200, and 800 m isobaths.

the frequency of eddy occurrence increases substantially over and to the northeast of the Charleston Bump, ranging from 15 to 20% for cyclonic eddies and from 15 to 25% for anticyclones. A map of eddy polarity (Figure 2c), defined as the difference between the frequency of occurrence of anticyclonic and cyclonic eddies divided by the total frequency of eddy occurrence ([*Chaigneau et al*., 2009], so that negative values indicate a dominance of cyclones), reveals a predominance of anticyclones inshore of the 800 m isobath and of cyclonic eddies offshore.

[12] The general characteristics of eddies also vary spatially and with polarity. The amplitude of cyclonic eddies inshore of the 800 m isobath increases substantially to the north of the Charleston Bump (Figure 3). In the shallower areas south of the topography perturbation, the average eddy amplitude is smaller than 4 cm (Figure 4b). The average amplitude increases sharply between 31°N and 32°N and remains large to the north of 32°N inshore of the 800 m isobath, at about 12–14 cm. There are several cyclonic eddies to the northeast of the Charleston Bump, however, with amplitudes as large as 30 cm in a band that extends from 77.8°W, 31.9°N to 73.7°W, 35.6°N. This contrasts with the distribution of the amplitude of anticyclonic eddies (Figure 5). Inshore of the 800 m isobath, the average amplitude of anticyclones also increases around the Charleston Bump, but it decreases again to the north of 32°N (Figure 4b). To the north of the Bump, very few eddies have amplitude in excess of 15 cm. The area with the highest eddy amplitude inshore of the 800 m isobath coincides with the area with the highest frequency of occurrence of anticyclonic

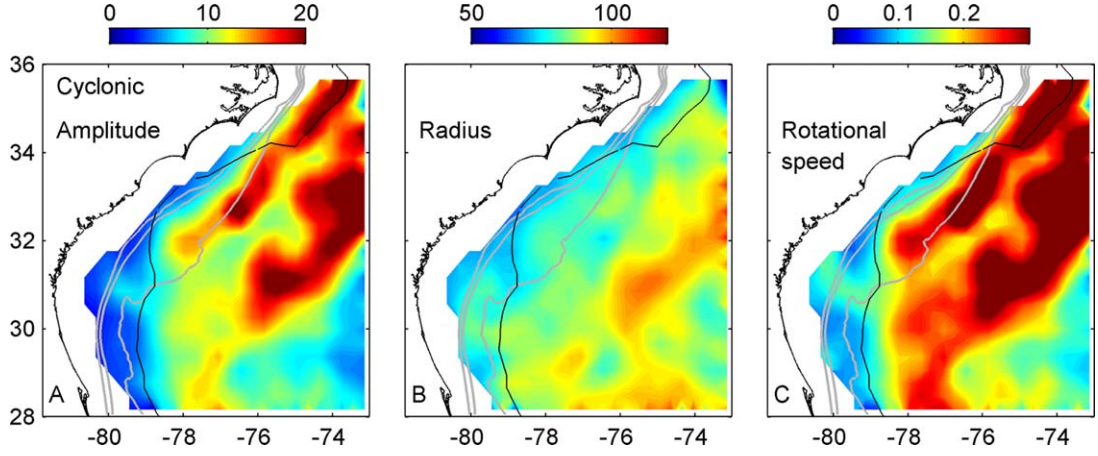

Figure 3. (a) Mean amplitude (cm), (b) radius (km), and (c) rotational speed (m s^{-1}) for all cyclonic eddies with lifetime ≥4 weeks that passed through each 0.35° × 0.35° region. The 60, 200, and 800 m isobaths are shown in gray. The black line shows the contour where the frequency of occurrence of cyclonic eddies is 10%. Note that since few eddies were observed to the west of the contour, statistics are less reliable in that area. Maximum values in the color scale were chosen to reveal as much as possible of the horizontal structure for each quantity.

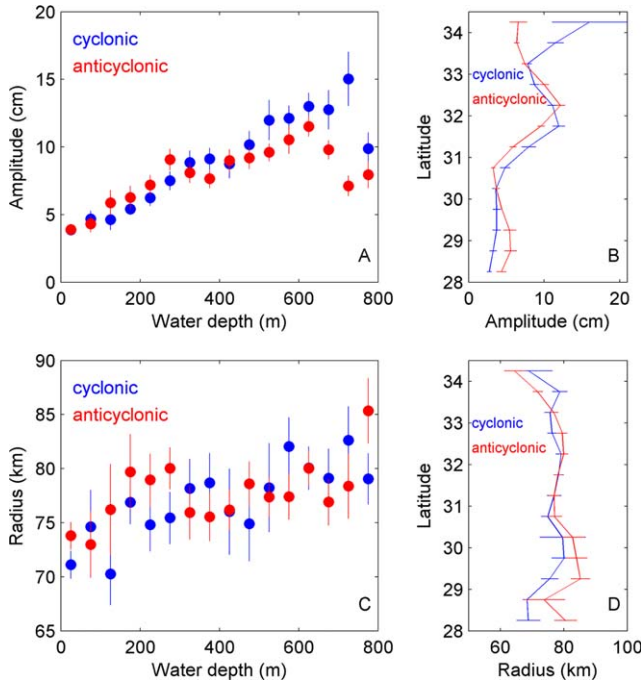

Figure 4. (a and b) Binned scatterplots of amplitude and (c and d) radius of cyclonic (blue) and anticyclonic (red) eddies with lifetime ≥4 weeks as a function of water depth or latitude. Only eddies found inshore of the 800 m isobath are used in the computation. The error bars represent the ±1 standard error of the mean within each bin.

eddies (Figure 2). Regardless of eddy polarity, average amplitudes increase with water depth, from <5 cm inshore of the 100 m isobath to 10–15 cm near the 800 m isobath (Figure 4a). A histogram of the number of cyclonic and anticyclonic eddies observed inshore of the 800 m isobath as a function of eddy amplitude reveals that small amplitude eddies are more often anticyclones, while no preference for a particular eddy polarity is observed for large amplitude eddies (>20 cm) (Figure 6a). It is important to point out, though, that very few eddies inshore of the 800 m isobath have amplitude larger than 20 cm. Cumulative eddy counts reveal that there are 0.55 cyclones and 0.66 anticyclones inshore of the 800 m isobath per snapshot (once per week).

[13] In contrast to eddy amplitude, the spatial pattern of eddy radius distribution does not vary substantially with polarity. Large eddies with radius exceeding ~100 km are only observed far from the coast (Figures 3 and 5). Inshore of the 800 m isobath, the average radius increases slightly with increasing water depth, from about 70 km near the coast to 80 km offshore, and no substantial alongshore variability is observed (Figures 4c and 4d). In those shallower regions, the vast majority of eddies have radius smaller than 120 km (Figure 6b). Eddies with radius between 60 and 100 km are more frequently anticyclones. Repeating these analyses using the spatial scale based on the area of the eddy inside the SLA contour where the average geostrophic velocity around the eddy is maximum produces results qualitatively similar. A least square fit reveals that, in that case, the spatial scale is reduced to 61% of the original values shown in Figures 3 and 5 for the eddy radius. The distribution of eddy rotational speed is very similar to the distribution of eddy amplitude for both cyclones and anticyclones. For cyclones, eddy rotational speeds inshore of the 800 m isobath are about 0.1–0.15 m s^{-1} to the south of the Charleston Bump, increasing to 0.2–0.5 m s^{-1} to the northeast of the Bump (Figure 3). For anticyclonic eddies, large rotational speeds inshore of the 800 m isobath are restricted to the area surrounding the Bump, decreasing substantially to the north or south of it (Figure 5).

[14] The temporal evolution of the average number of eddies observed in each month in the SAB inshore of the 800 m isobath reveals that seasonal variability is small (Figure 7a). Differences in the number of anticyclones and cyclones between months are likely not significant, perhaps

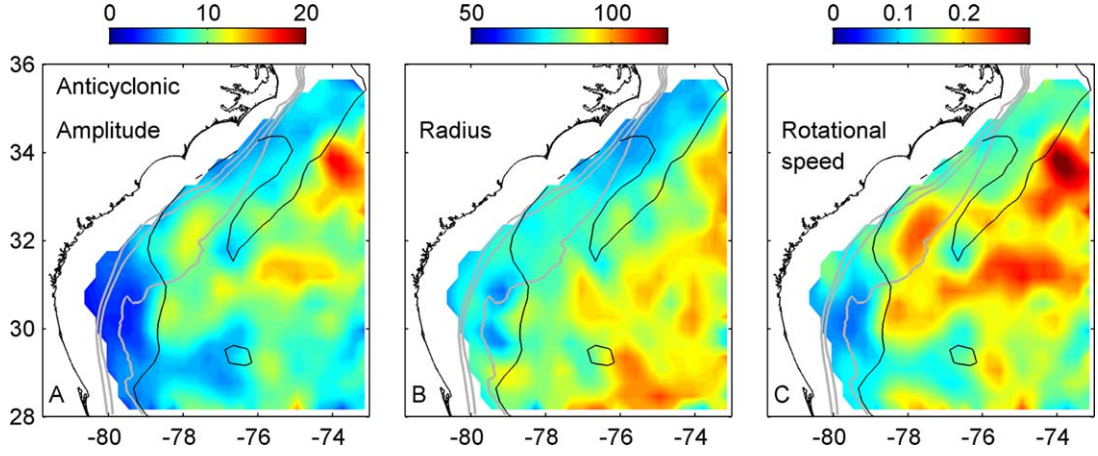

Figure 5. (a) Mean amplitude (cm), (b) radius (km), and (c) rotational speed (m s^{-1}) for all anticyclonic eddies with lifetime ≥4 weeks that passed through each 0.35° × 0.35° region. The 60, 200, and 800 m isobaths are shown in gray. The black line shows the contour where the frequency of occurrence of anticyclonic eddies is 10%. Note that since few eddies were observed to the west of the contour, statistics are less reliable in that area. Maximum values in the color scale were chosen to reveal as much as possible of the horizontal structure for each quantity.

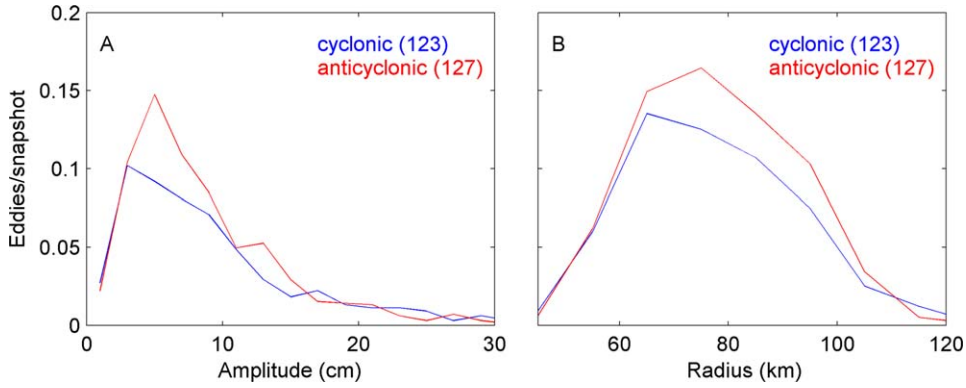

Figure 6. Distributions of the (a) amplitudes and (b) radius of eddies with lifetime ≥4 weeks. Only eddies found inshore of the 800 m isobath are used in the computation. Number of eddies are shown in parentheses.

with a few exceptions. There is substantial interannual variability in eddy occurrence, however, with the number of cyclonic eddies observed per month ranging from 0.7 to 4.1 and the number of anticyclones varying between 1.3 and 4.7 (Figure 7b). Interestingly, the number of cyclones and anticyclones seem to vary out of phase, at least during certain periods. Both time series are significantly correlated (at the 95% confidence level) with the Gulf Stream transport off Florida (~26.5°N). The time-lagged correlation peaks with a lag of 5 months (transport time series preceding time series of number of eddies per month), and is positive ($r = 0.46$) for cyclonic eddies, and negative ($r = -0.37$) for anticyclones. The time series of the number of eddies per month are not significantly correlated (at the 95% confidence level) with alongshelf wind stress anomalies ($r = 0.22$ for cyclones, $r = 0.01$ for anticyclones).

3.2. Eddy Generation and Propagation

[15] Not all eddies shown in the previous section were generated in the South Atlantic Bight. Some of them were generated farther offshore and propagated westward into the study region. On average, 2.45 eddies are generated in the area each month. The spatial distribution of the number of eddies actually generated in the SAB per year, in 1° × 1° boxes, is shown in Figure 8. The frequency of eddy generation is enhanced between the 800 m and ~1000 m isobaths to the south of 31°N, and between the 60 m and 600–800 m isobaths to the northeast of 31°N. Maximum eddy generation frequency is observed around the Charleston Bump, where about 1.6 eddies are generated each year. The time series of the number of cyclonic and anticyclonic eddies generated in each month around the Charleston Bump are not significantly correlated with alongshelf wind stress anomalies. Offshore of the 1000 m isobath, the number of eddies generated decrease substantially.

[16] There is a tendency for eddies generated in the SAB region to propagate westward for several hundred kilometers (Figures 9a and 9b), with 58% of the cyclones and 54% of the anticyclones propagating to the west. Cyclonic eddies seem to propagate farther onshore than anticyclones. Of the westward propagating eddies, 57% of the cyclones and 49% of the anticyclones also propagate northward. Of eddies that move eastward, on the other hand, 83% of the cyclones and 74% of the anticyclones propagate northward. We also investigated propagation characteristics of eddies generated inshore of the 800 m isobath (Figures 9c and 9d). In that case, the majority of eddies (58% of cyclones and 50% of anticyclones) propagate northeastward. If only

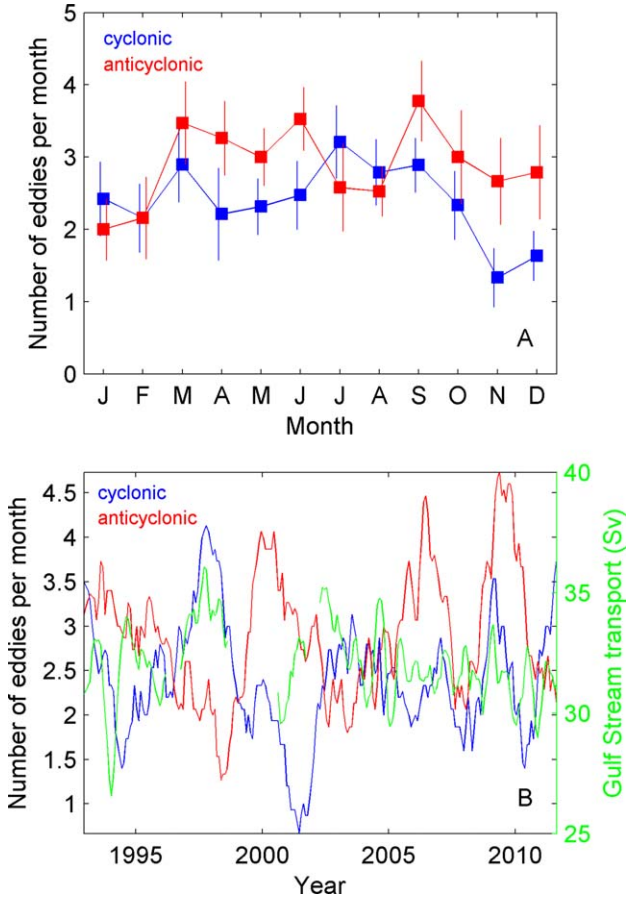

Figure 7. (a) Average number of cyclonic (blue) and anticyclonic (red) eddies with lifetime ≥4 weeks found in each month inshore of the 800 m isobath in the SAB. The error bars represent the ±1 standard error of the mean within each month. (b) Interannual variability in the number of eddies observed in each month is shown in bottom. Time series have been smoothed with a 15 month running mean. Gulf Stream transport (Sv) at ~26.5°N is shown in green.

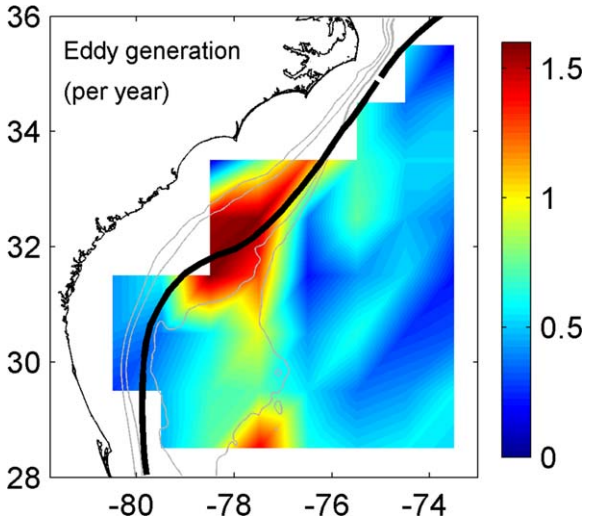

Figure 8. The number of eddies with lifetime ≥4 weeks generated per year for 1° × 1° boxes. Thick black line is a contour of mean dynamic topography, which shows the long-term average position of the core of the Gulf Stream. The 60, 200, 800, and 1000 m isobaths are shown in gray.

eddies that propagate at least 100 km from the point of generation are considered, the fraction of cyclones and anticyclones that propagate northeastward increases to 74% and 78%, respectively. The predominant angle of eddy propagation roughly coincides with the average direction of the mean flow in the Gulf Stream to the northeast of the Charleston Bump, where most eddies are generated.

[17] In order to quantify the nonlinearity of the eddies, we computed the nondimentional ratio U/c, where U is the maximum rotational speed and c is the translation speed of the eddy estimated at each point along the trajectory [*Chelton et al*., 2007, 2011b]. When $U/c > 1$, the speed of rotation exceeds the speed of propagation, and eddies can effectively trap water inside and transport water properties such as heat, salt, and nutrients along their tracks [*Samelson and Wiggins*, 2006; *Chelton et al*., 2011b]. Only eddies that at some point in their trajectory are found inshore of the 800 m isobath are used in the analyses. The vast majority of cyclones and anticyclones are characterized by $U/c > 1$ (Figure 10b). The ratio exceeds 5.7 and 6.3 for 50% of cyclones and anticyclones, respectively. The cumulative percentage of eddies as a function of the advective nonlinear parameter is similar for cyclonic and anticyclonic eddies. By tracking the total water depth along the trajectory of each individual eddy, it is estimated that 44% of cyclonic eddies and 52% of anticyclones remain inshore of the 800 m isobath for over 28 days (Figure 10a). Note that these are lower-bound estimates, since if an eddy is observed inshore of the 800 m isobath in three snapshots 7 days apart, it is assumed here that it remained in that region for 14 days.

[18] Examples of trajectories of cyclonic and anticyclonic nonlinear eddies are shown in Figure 11. Circles show eddy centroids, color coded by the advective nonlinear parameter. Black squares show initial position of the eddies. In all plots, only once the nonlinear parameter is smaller than 1, and values of U/c exceed 6 approximately 33% of the time. The examples show that both cyclonic and anticyclonic nonlinear eddies can travel large distances with substantial changes in water depth. That is true for eddies traveling onshore as well as for those traveling offshore. We also tracked the total water depth change along trajectories for all eddies that are found inshore of the 800 m isobath at some point in their history (Figure 12). Of those, 63% travel onshore (i.e., toward shallower waters), while 37% travel offshore (i.e., toward deeper waters). The majority of eddies, regardless of the direction of propagation, experience bathymetric changes smaller than 500 m. For some eddies, however, large bathymetric changes are observed along their trajectories. For eddies propagating onshore, 15.4% propagate over water depth changes exceeding 1000 m, while 7% exceed 3000 m water depth changes. For eddies moving offshore toward deeper regions, the percentage that have trajectories with bathymetric changes exceeding 1000 and 3000 m are 11.8% and 1%, respectively.

4. Discussion and Conclusions

[19] Sea level anomaly (SLA) altimeter observations spanning a 19 year period were used to characterize the distribution and properties of cyclonic and anticyclonic eddies in the South Atlantic Bight (SAB) using the eddy detection and eddy tracking algorithms described in *Chelton et al*. [2011b]. Comparisons of satellite observations with data from multiple tide gauges along the SAB (Figure 1) reveal that reliable observations can be obtained for locations farther than 40 km from the coast. Over the 19 year period investigated here, 744 eddies that could be tracked for at least 4 weeks were observed in the area. Many more could be tracked for 3 weeks or less, but those were discarded to reduce the risk of spurious eddies arising from noise in the SLA fields. Of the 744 eddies detected, 250 were observed inshore of the 800 m isobath at some point in their time history (i.e., they were either generated inshore of the 800 m or they were generated farther offshore and propagated onshore). Because those eddies can stay in those relatively shallow waters for several weeks (Figure 10a), approximately 1.2 eddies can be observed per week inshore of the 800 m isobath, with a slight preference for anticyclones over cyclones (Figures 2 and 7). Downstream (i.e., in the direction of the mean flow of the Gulf Stream) of the Charleston Bump, eddies are observed almost 50% of the time (Figure 2), especially between 32°N and 34°N. In that area, high frequency of eddy occurrence can even be observed over the outer shelf (Figure 2). These likely represent lower bound estimates for the frequency of eddy occurrence in the region, since eddies with e-folding scales smaller than 0.4° are filtered out of the objective analyses procedure implemented by SSALTO/DUACS, while those between 0.4° and 0.6° are attenuated [*Chelton et al*., 2011b].

[20] The increase in the frequency of eddy occurrence over and downstream of the Charleston Bump is accompanied by an increase in eddy amplitude and rotational speed for both cyclonic and anticyclonic eddies (Figures 3–5). Eddy-topography interactions have been shown to be important in determining the evolution of eddies in other settings [e.g., *LaCasce*, 1998; *Hyun and Hogan*, 2008]. Using numerical model simulations, *Oey et al*. [1992] showed

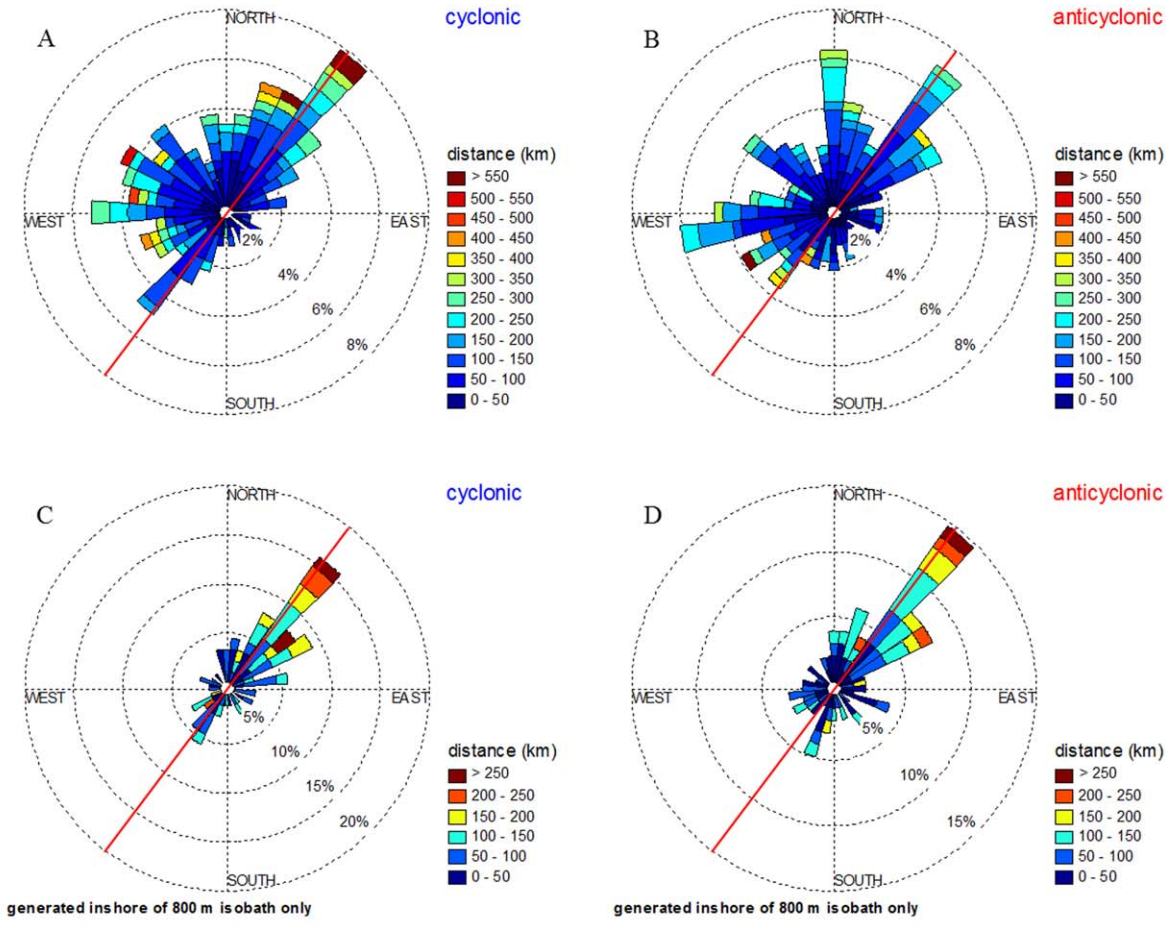

Figure 9. Direction of propagation of (left) cyclonic and (right) anticyclonic eddies generated in the (a and b) SAB and (c and d) inshore of the 800 isobath with lifetime ≥4 weeks, color coded by propagation distance. Length of spokes shows frequency of time that eddies propagate in a particular direction. The red line indicates the direction of the mean flow of the Gulf Stream to the northeast of the Charleston Bump (from Figure 1).

that bottom irregularities in the form of a bump can lead to significant increases in western boundary current variability. In particular, their numerical simulations of the circulation in the SAB indicate a peak in surface elevation variability and eddy kinetic energy just downstream of the Charleston Bump, which is due to meanders developed as a

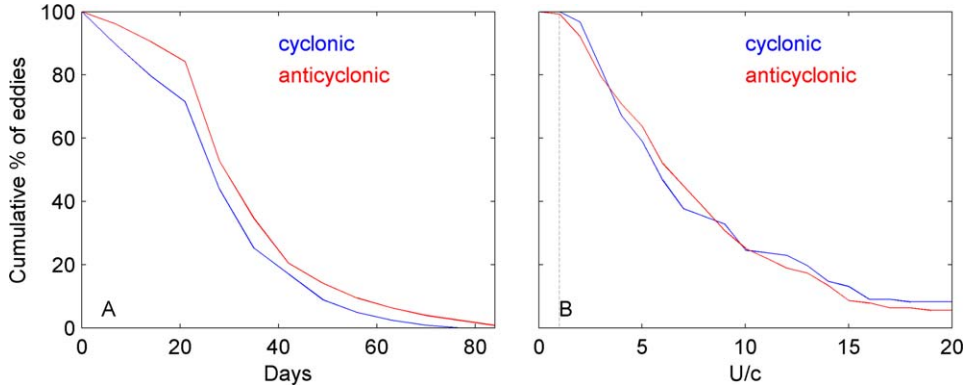

Figure 10. Distributions of (a) number of consecutive days an eddy is located inshore of the 800 m isobath and (b) advective nonlinearity parameter for eddies with lifetime ≥4 weeks. Only eddies that are found inshore of the 800 m isobath at some point in their history are used in the computation.

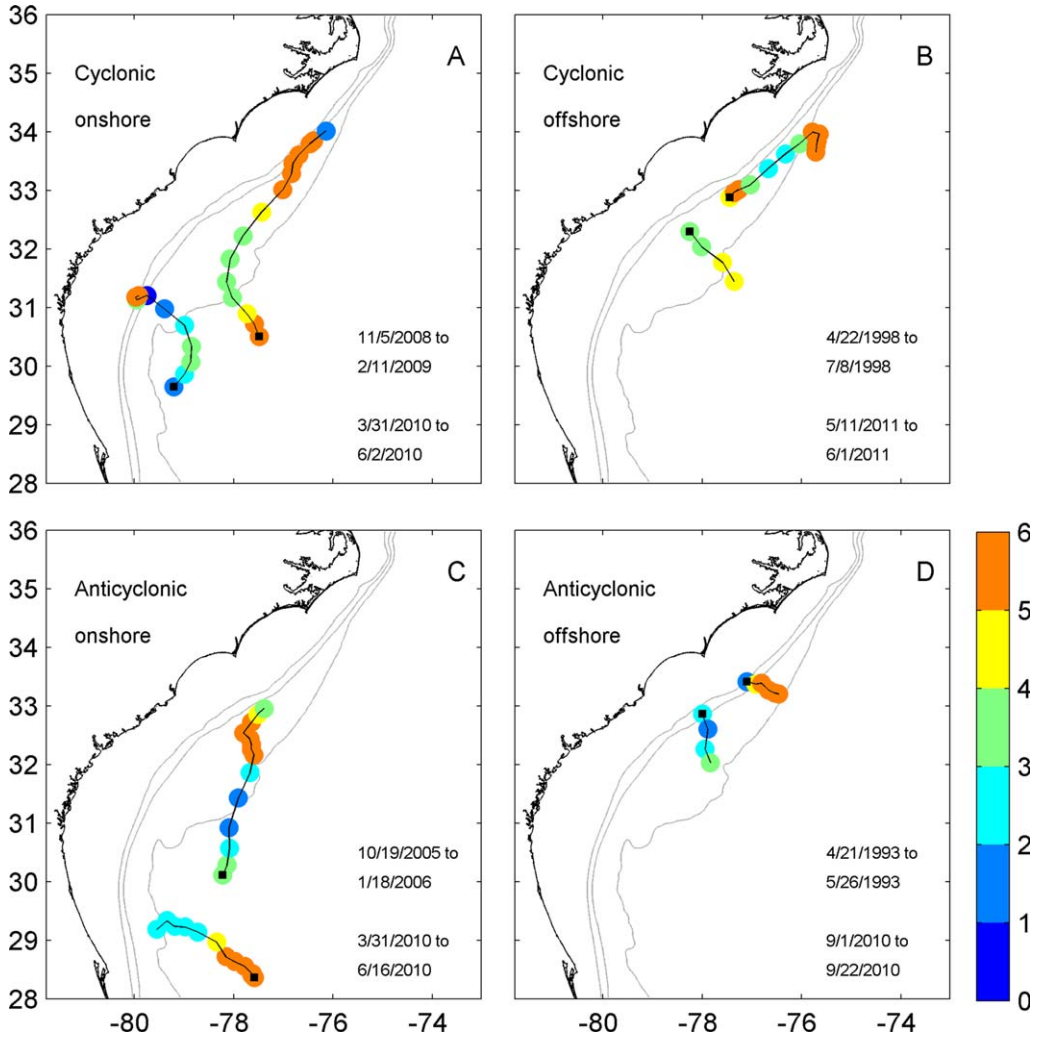

Figure 11. Examples of trajectories of cyclonic and anticyclonic eddies in the SAB with lifetime $\geq$4 weeks. Circles are eddy centroids shown every 7 days, color coded by advective nonlinearity parameter. Small black squares show initial eddy position. Eddies that move onshore are shown on the left, while eddies that move toward deeper water are shown on the right. The 60, 200, and 800 m isobaths are shown in gray. Initial and end dates of trajectories are shown on each panel. Dates shown on top are for trajectories that reach farther north. Advective nonlinearity parameters larger than 6 are shown in orange to reveal as much as possible of the horizontal structure.

result of flow deflection at the topography perturbation. Increase in the magnitude of Gulf Stream meanders downstream of the Bump has also been observed in SST imagery [e.g., *Bane and Brooks*, 1979; *Bane et al*., 1981]. This is consistent with the increase in frequency and amplitude of cyclonic and anticyclonic eddies at and downstream of the Bump (Figures 2 and 4b). Interestingly, while anticyclones with high amplitude are restricted to the Bump area (Figure 5), high amplitude cyclones can also be found to the northeast of the topography perturbation (Figure 3), in a line that is roughly parallel to the mean position of the Gulf Stream [*Bane and Brooks*, 1979]. It is possible, therefore, that cyclonic eddies are generated (e.g., Figure 8) or amplified over the Bump, and then advected northeastward by the mean flow of the western boundary current (Figure 9). It is not clear, however, why a similar string of high amplitude anticyclonic eddies is not observed to the northeast of the perturbation. *Lee et al*. [1991] reported that cyclonic, cold-core eddies embedded in the Gulf Stream front along the North Carolina outer shelf occur when the Gulf Stream meanders offshore. They also report that the cold-core eddies move northward at the same speed as the meanders. The northeastward moving eddies reported by *Lee et al*. [1991] are likely different features than those reported here, though, since they indicate that those eddies can have downstream dimensions of up to 300 km, they have a lifespan of only up to 3 weeks (compared to a minimum lifespan of 4 weeks for the eddies reported here) and they seem to propagate faster.

[21] The possible influence of the Gulf Stream deflecting eddies in the study region can also be seen by comparing the propagation characteristics of eddies in the SAB with the characteristics of eddy propagation based on global analyses. Previous studies have shown that the great

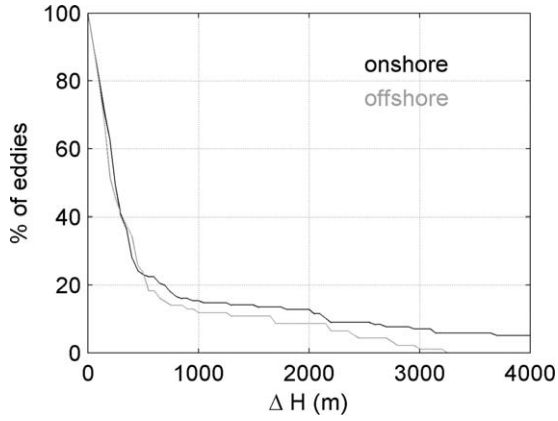

Figure 12. Cumulative histogram of bathymetric changes experienced by eddies with lifetime ≥4 weeks moving onshore (black) and offshore (gray). Only eddies that are found inshore of the 800 m isobath at some point in their history are used in the computation.

majority of eddies worldwide propagate westward [e.g., *Lee and Mellor*, 2003; *Morrow et al*., 2004; *Chelton et al*., 2007, 2011b]. In the SAB, however, only 58% and 54% of the cyclonic and anticyclonic eddies propagate to the west, respectively (Figures 9a and 9b). The relatively large fraction of eddies that move eastward is likely associated with the presence of the Gulf Stream, which flows predominantly in a northeastward direction to the north of 31°N (see also Figure 1). Indeed, the large majority of cyclones and anticyclones that propagate eastward also propagate northward. Additionally, while *Chelton et al*. [2011b] showed that globally 55% and 30% of the westward propagating cyclones and anticyclones, respectively, also propagate poleward, the fraction of westward propagating eddies in the SAB that also move poleward is larger at 57% and 49% for cyclones and anticyclones, respectively. The fact that many more eddies, in particular anticyclones, propagate poleward in the SAB than in global observations could be the result of the interaction of the eddies with the western boundary current. Finally, if only eddies generated inshore of the 800 m isobath that propagate at least 100 km are considered, analyses indicate that about 75% of them propagate to the northeast approximately along the main axes of the Gulf Stream (Figures 9c and 9d). This is against the direction of propagation of coastally trapped waves, supporting the idea that their trajectory is influenced by the mean flow of the Gulf Stream.

[22] In contrast to eddy amplitude and rotational speed, no significant change in eddy radius is observed around the Charleston Bump (Figure 4b). It is possible that this may have been influenced by the filtering effect of limited spatial resolution of the SLA field. The small increase in eddy radius observed as a function of water depth (Figure 4c) may be at least partially related to variations in the first baroclinic Rossby radius (R_i), which increases approximately linearly with water depth in the region (from ∼6.5 km at the 100 m isobath to ∼23 km at the 800 m isobath; $r^2 = 0.93$). The slope of the regression is quite different than the relationship between water depth and average radius (Figure 4c), however, suggesting that other factors may also be important.

[23] Gulf Stream eddies have long been associated with cross-isobath flow in the form of subsurface intrusions during summer [e.g., *Atkinson et al*., 1987; *Lee et al*., 1991; *Aretxabaleta et al*., 2006], particularly if coincident with upwelling favorable winds [e.g., *Lee and Pietrafesa*, 1987; *Hyun and He*, 2010; *Castelao*, 2011]. In that case, the water transported onto the shelf is upwelled in the cold core of frontal eddies, impacting shelf hydrography and biological productivity [*Paffenhofer et al*., 1987]. The recent availability of high resolution SLA fields constructed by merging measurements from simultaneously operating altimeters [*Ducet et al*., 2000; *Le Traon et al*., 2003; *Chelton et al*., 2011b] revealed that the vast majority of eddies of either polarity in the SAB are characterized by advective nonlinear parameter $(U/c) > 1$ (Figure 10b). This implies that they can trap and transport water within their interior as they propagate [*Samelson and Wiggins*, 2006; *Chelton et al*., 2011b]. Off the coast of Alaska, for example, eddies have been shown to carry excess nutrients and iron in their core waters into pelagic regions as they propagate away from the continental margin [*Crawford et al*., 2007]. When nonlinear eddies propagate across isobaths in the SAB, as in the examples shown in Figure 11, they can potentially transport water and any material contained in their interior onshore or offshore for large distances. Note that this is a different mechanism for cross-isobath transport than the eddy-induced subsurface intrusions reported previously [e.g., *Lee et al*., 1991]. The present analysis reveals that almost 20% of all eddies that at some point in their trajectories are found inshore of the 800 m isobath in the SAB have crossed isobaths with a bathymetric change of at least 1000 m (Figure 12). Therefore, nonlinear eddies of either polarity can potentially contribute substantially to shelf-slope exchange of heat, salt, nutrients and carbon in the SAB. The importance of this cross-isobath exchange mechanism possibly does not vary seasonally, but may vary from year to year in relation to interannual variability in eddy activity (Figure 7).

[24] The mechanism responsible for the interannual variability in the number of cyclonic and anticyclonic eddies found in each month inshore of the 800 m isobath in the SAB is currently unknown. We note that the time series of the number of eddies found in each month are not correlated with alongshelf wind stress anomalies, but they are significantly correlated with the monthly averaged transport of the Gulf Stream farther south (Figure 7b). The correlation indicates a predominance of cyclonic eddies during periods when the Gulf Stream transport is intensified. If we assume that shelf currents are uncorrelated to the strength of the Gulf Stream (a reasonable assumption, since shelf currents are primarily driven by local winds [*Lee et al*., 1991]), intensifications in the Gulf Stream are accompanied by intensifications in the velocity shear between the boundary current and the shelf. Therefore, it is possible that the decrease in the number of anticyclones and the increase in the number of cyclones inshore of the 800 m isobath during periods of transport intensification are related to the simultaneous increase in the cyclonic shear on the shoreward side of the Gulf Stream. This would imply a direct influence of the large scale circulation on eddy dynamics in the SAB. We note that the time series of interannual variability in eddy occurrence inshore of the 800 m isobath is not

correlated to the Gulf Stream transport if only eddies that have been generated offshore of the 800 m isobath and propagated onshore are used in the computation. This provides further support to the interpretation given above.

[25] Another possibility is that variations in the frequency of occurrence of cyclonic and anticyclonic eddies inshore of the 800 m isobath is related to the position of the Gulf Stream. Previous studies [e.g., *Bane and Dewar*, 1988] have shown that the seaward deflection of the Gulf Stream at the Charleston Bump has a bimodal character, oscillating between a weakly deflected state, where the shoreward Gulf Stream SST front remains inshore of the 600 m isobath between the Charleston Bump and Cape Hatteras, and a strongly deflected state, where the front is located several tens of kilometers offshore of the 600 m isobath. *Bane and Dewar* [1988] showed that the Gulf Stream meander field downstream of the bump differs between the two states of deflection, which suggests that the bimodality in deflections could potentially influence the relative frequency of cyclones and anticyclones in the region. Previous observations reveal, however, that the Gulf Stream remains in each deflected state for a matter of a few months [*Bane et al*., 1981; *Brooks and Bane*, 1981; *Hood and Bane*, 1983; *Bane and Dewar*, 1988], while the number of cyclones and anticyclones observed inshore of the 800 m isobath in the SAB clearly vary on a multiyear time scale (Figure 7b). Additionally, the position of the Gulf Stream shoreward SST front in the deflection region undergoes a season oscillation [*Olson et al*., 1983], so that the strongly deflected state occurs preferentially during fall and winter [*Bane and Dewar*, 1988], while no significant seasonal variability is observed in the number of eddies of either polarity observed inshore of the 800 m (Figure 7a). Therefore, although we cannot rule out that possibility, it seems unlikely that the position of the Gulf Stream plays a dominant role setting the observed interannual variability in eddy polarity inshore of the 800 m isobath in the SAB.

[26] The spatial distribution of the frequency of eddy occurrence (Figure 2) presents some puzzling features. It is not clear, for example, why the frequency of occurrence of both cyclonic and anticyclonic eddies is substantially reduced at 76–77°W, 29–30°N. The region is characterized by major topographic variations (Figure 1), with the total water depth changing from 5000 m to 1500 m over a distance of 30 km. The area just seaward of the 800 m isobath to the northeast of 31°N is also characterized by weak eddy occurrence. One could argue, however, particularly for the case of anticyclones (Figure 2b), that the frequency of eddy occurrence decreases toward the coast before the 800 m isobath is reached everywhere in the SAB, except at and downstream of the Charleston Bump. Based on that interpretation, eddy occurrence seaward of the 800 m isobath to the northeast of 31°N would not be anomalously weak. Instead, it would appear weak because the frequency of eddy occurrence is strongly intensified farther inshore over the Bump. Further investigating the controls of the observed spatial variability in eddy occurrence (Figure 2) awaits future studies.

[27] In summary, SLA observations were used to quantify the frequency of occurrence and to characterize the properties of cyclonic and anticyclonic eddies in the South Atlantic Bight. Inshore of the 800 m isobath, eddies are more frequently observed over and just downstream of the Charleston Bump, a major topographic feature where eddy amplitudes are also larger. There is a clear tendency for eddies to propagate toward the west or to the northeast along the main axis of the Gulf Stream. Since most eddies are nonlinear and several of them experience substantial bathymetric changes along their trajectory, they can potentially serve as an efficient cross-isobath transport mechanism in the South Atlantic Bight.

[28] **Acknowledgments.** We thank Alexis Chaigneau and two anonymous reviewers for their thoughtful and very helpful comments and suggestions, which led to a greatly improved manuscript. We gratefully acknowledge support by NASA Ocean Surface Topography Mission through grant NNX13AD80G. We thank CLS/AVISO for distributing the SSALTO/DUACS altimeter data used here, and the University of Hawaii Sea Level Center for distributing the tide gauge observations. We also thank NOAA for making Florida Current transport observations publicly available through the Western Boundary Time Series project.

References

Aretxabaleta, A., J. Nelson, J. Blanton, H. Seim, F. Werner, J. Bane, and R. Weisberg (2006), Cold event in the South Atlantic Bight during summer of 2003: Anomalous hydrographic and atmospheric conditions, *J. Geophys. Res.*, *111*, C06007, doi:10.1029/2005JC003105.

Atkinson, L. P., and J. O. Blanton (1986), Processes that affect stratification in shelf waters, in *Baroclinic Processes on Continental Shelves, Coastal Estuarine Sci. Ser*., vol. *3*, edited by C. N. Mooers, pp. 117–130, AGU, Washington, D. C.

Atkinson, L. P., J. Blanton, and E. Haines (1978), Shelf flushing rates based on the distribution of salinity and freshwater in the Georgia Bight, *Estuarine Coastal. Mar. Sci.*, *7*, 465–472.

Atkinson, L. P., T. N. Lee, J. O. Blanton, and G. A. Paffenhofer (1987), Summer upwelling on the southeastern continental shelf of the USA during 1981: Hydrographic observations, *Prog. Oceanogr.*, *19*, 231–266.

Bane, J., and D. Brooks (1979), Gulf Stream meanders along the continental margin from the Florida Straits to Cape Hatteras, *Geophys. Res. Lett.*, *6*, 280–282.

Bane, J., and W. Dewar (1988), Gulf Stream bimodality and variability downstream of the Charleston Bump, *J. Geophys. Res.*, *93*, 6695–6710.

Bane, J., D. Brooks, and K. Lorenson (1981), Synoptic observations of the three-dimensional structure and propagation of Gulf Stream meanders along the Carolina Continental Margin, *J. Geophys. Res.*, *86*, 6411–6425.

Blanton, J., and L. Pietrafesa (1978), Flushing of the continental shelf south of Cape Hatteras by the Gulf Stream, *Geophys. Res. Lett.*, *5*, 495–498.

Brooks, D., and J. Bane (1981), Gulf Stream fluctuations and meanders over the Onslow Bay upper continental slope, *J. Phys. Oceanogr.*, *11*, 247–256.

Castelao, R. (2011), Intrusions of Gulf Stream waters onto the South Atlantic Bight shelf, *J. Geophys. Res.*, *116*, C10011, doi:10.1029/2011JC007178.

Chaigneau, A., A. Gizolme, and C. Grados (2008), Mesoscale eddies off Peru in altimeter records: Identification algorithms and eddy spatio-temporal patterns, *Prog. Oceanogr.*, *79*, 106–119.

Chaigneau, A., G. Eldin, and B. Dewitte (2009), Eddy activity in the four major upwelling systems from satellite altimetry, *Prog. Oceanogr.*, *83*, 117–123.

Chelton, D., P. Gaube, M. Schlax, J. Early, and R. Samelson (2011a), The influence of nonlinear mesoscale eddies on near-surface oceanic chlorophyll, *Science*, *334*, 328–332.

Chelton, D., M. Schlax, and R. Samelson (2011b), Global observations of nonlinear mesoscale eddies, *Prog. Oceanogr.*, *91*, 167–216.

Chelton, D. B., M. G. Schlax, R. M. Samelson, and R. A. de Szoeke (2007), Global observations of large oceanic eddies, *Geophys. Res. Lett.*, *34*, L15606, doi:10.1029/2007GL030812.

Crawford, W., P. Brickley, and A. Thomas (2007), Mesoscale eddies dominate surface phytoplankton in northern Gulf of Alaska, *Prog. Oceanogr.*, *75*, 287–303.

Ducet, N., P. Le Traon, and G. Reverdin (2000), Global high resolution mapping of ocean circulation from TOPEX/POSEIDON and ERS-1/2, *J. Geophys. Res.*, *105*, 19,477–19,498.

Gruber, N., et al. (2011), Eddy-induced reduction of biological production in eastern boundary upwelling systems, *Nat. Geosci.*, *4*, 787–792.

Hood, C., and J. Bane (1983), Subsurface energetics of the Gulf Stream cyclonic frontal zone off Onslow Bay, north Carolina, *J. Geophys. Res.*, *88*, 4651–4662.

Hyun, K. H., and R. He (2010), Coastal upwelling in the South Atlantic Bight: A revisit of the 2003 cold event using long term observations and model hindcast solutions, *J. Mar. Syst.*, *83*, 1–13.

Hyun, K. H., and P. J. Hogan (2008), Topographic effects on the path and evolution of Loop Current Eddies, *J. Geophys. Res.*, *113*, C12026, doi:10.1029/2007JC004155.

Kundu, P., J. Allen, and R. Smith (1975), Modal decomposition of the velocity field near the Oregon coast, *J. Phys. Oceanogr.*, *5*, 683–704.

LaCasce, J. H. (1998), A geostrophic vortex over a slope, *J. Phys. Oceanogr.*, *28*, 2362–2380.

Lagerloef, G. S. E. (1992), On the Point Arena Eddy: A recurring summer anticyclone in the California Current, *J. Geophys. Res.*, *97*, 12,557–12,568.

Lee, H.-C., and G. L. Mellor (2003), Numerical simulation of the Gulf Stream System: The Loop Current and the deep circulation, *J. Geophys. Res.*, *108*(C2), 3043, doi:10.1029/2001JC001074.

Lee, M., and R. Williams (2000), The role of eddies in the isopycnic transfer of nutrients and their impact on biological production, *J. Mar. Res.*, *58*, 895–917.

Lee, T. N., and L. P. Atkinson (1983), Low-frequency current and temperature variability from Gulf Stream frontal eddies and atmospheric forcing along the southeast U.S. outer continental shelf, *J. Geophys. Res.*, *88*, 4541–4568.

Lee, T. N., and L. Pietrafesa (1987), Summer upwelling on the southeastern continental shelf of the USA during 1981: Circulation, *Prog. Oceanogr.*, *19*, 267–312.

Lee, T. N., L. P. Atkinson, and R. Legeckis (1981), Observations of a Gulf Stream frontal eddy on the Georgia continental shelf, April 1977, *Deep Sea Res., Part A*, *18*, 347–348.

Lee, T. N., J. A. Yoder, and L. P. Atkinson (1991), Gulf Stream frontal eddy influence on productivity on the southeast U.S. continental shelf, *J. Geophys. Res.*, *96*, 22,191–22,205.

Le Traon, P., Y. Faugère, F. Hernandes, J. Dorandeau, F. Mertz, and M. Ablain (2003), Can we merge Geosat follow-on with TOPEX/Poseidon and ERS-2 for an improved description of the ocean circulation?, *J. Atmos. Oceanic Technol.*, *20*, 889–895.

McGillicudy, D., et al. (1998), Influence of mesoscale eddies on new production in the Sargasso Sea, *Nature*, *394*, 263–266.

Morrow, R., F. Birol, D. Griffin, and J. Sudre (2004), Divergent pathways of cyclonic and anti-cyclonic ocean eddies, *Geophys. Res. Lett.*, *31*, L24311, doi:10.1029/2004GL020974.

Oey, L. T. Ezer, G. Mellor, and P. Chen (1992), A model study of "bump" induced western boundary current variabilities, *J. Mar. Syst.*, *3*, 321–342.

Olson, D. B., O. B. Brown, and S. R. Emmerson (1983), Gulf Stream frontal statistics from Florida Straits to Cape Hatteras derived from satellite and historical data, *J. Geophys. Res.*, *88*, 4569–4577.

Oschlies, A., and V. Garçon (1998), Eddy-induced enhancement of primary production in a model of the North Atlantic Ocean, *Nature*, *394*, 266–269.

Paffenhofer, G., B. Sherman, and T. Lee (1987), Summer upwelling on the southeastern continental shelf of the U.S.A. during 1981, abundance, distribution and patch formation of zooplankton, *Prog. Oceanogr.*, *19*, 403–436.

Pascual, A., Y. Faugere, G. Larnicol, and P. Le Traon (2006), Improved description of the ocean mesoscale variability by combining four satellite altimeters, *Geophys. Res. Lett.*, *33*, L02611, doi:10.1029/2005GL024633.

Robinson, A. R. (Ed.) (1983), *Eddies in Marine Science*, 609 pp., Springer, New York.

Samelson, R. M., and S. Wiggins (2006), *Lagrangian Transport in Geophysical Jets and Waves: The Dynamical Systems Approach*, 147 pp., Springer, New York.

Saraceno, M., P. T. Strub, and P. M. Kosro (2008), Estimates of sea surface height and near-surface alongshore coastal currents from combinations of altimeters and tide gauges, *J. Geophys. Res.*, *113*, C11013, doi:10.1029/2008JC004756.

Volkov, D., G. Larnicol, and J. Dorandeu (2007), Improving the quality of satellite altimetry data over continental shelves, *J. Geophys. Res.*, *112*, C06020, doi:10.1029/2006JC003765.

Washburn, L., M. Swenson, J. Largier, P. Kosro, and S. Ramp (1993), Cross-shelf sediment transport by an anticyclonic eddy off northern California, *Science*, *261*, 1560–1564.